SPECIAL ISSUE RESEARCH ARTICLE

INTERNATIONAL JOURNAL OF
ENERGY RESEARCH WILEY

Comparison and study of the preparation methods for phosphor layer in nuclear battery

Tongxin Jiang[1] | Zhiheng Xu[1] | Xiaobin Tang[1,2] | Zicheng Yuan[1] |
Hongyu Wang[1] | Mingxin Bian[1]

[1]Department of Nuclear Science and Technology, Nanjing University of Aeronautics and Astronautics, Nanjing, China

[2]Key Laboratory of Nuclear Technology Application and Radiation Protection in Astronautics (Nanjing University of Aeronautics and Astronautics), Ministry of Industry and Information Technology, Nanjing, China

Correspondence
Xiaobin Tang, Department of Nuclear Science and Technology, Nanjing University of Aeronautics and Astronautics, Nanjing 211106, China.
Email: tangxiaobin@nuaa.edu.cn

Summary
This work investigated the preparation and optimization of phosphor layer for radioluminescent nuclear battery, and analyzed the property change of the phosphor after irradiation. ZnS:(Cu, Al) with grain size of 5 μm was selected as the phosphor material, and AlGaInP semiconductor was used as the photovoltaic unit. Monte Carlo modeling was used to simulate energy deposition, absorbed dose, penetration of β particles in the phosphor. The optimized coupling scheme of radioisotope sources and phosphor layer was obtained based on comparison particle penetration depth and the output power of radioluminescent nuclear battery. The phosphor layer with ^{60}Co γ-radiation enhanced the luminescence property up to 50% at the radiation dose of 871 kGy, which is considered as an optimized method of phosphor layer preparation. The radiation of 10 MeV electron was conducted to study the degradation based on the microscopic lattice characteristics, morphological changes, optical and electrical properties. Phosphors have excellent radiation resistance. The output power of nuclear batteries has only declined by 43% even when electron radiation dose reaches 8.56 MGy. The prospect for utilizing ZnS:(Cu, Al) phosphor as radiant energy conversion materials in nuclear battery was also discussed. Results provided an effective guideline for predict the service conditions of radioluminescent nuclear battery.

KEYWORDS
electron radiation, energy conversion, phosphor layer, radioluminescent nuclear battery

1 | INTRODUCTION

The nuclear battery is widely used in severe environments such as outer space and deep sea, because of its small size, light weight, long service life, and stable output power.[1-4] At present, miniaturized nuclear batteries mainly consist of decay particle conversion mechanism; however, radiovoltaic nuclear battery with direct conversion mode causes severe displacement damage of the semiconductor unit and shortens its service life.[5-8] The

radiation resistance of fluorescent materials is better than semiconductor materials.[9,10] Radioluminescent nuclear battery is a device that converts the decay particles of radioisotope sources into light and then forms an output current, which has inherent advantages for indirect energy conversion. Its structure is shown in Figure 1. Fluorescent materials are widely used in the radioluminescence field because of high luminescence intensity and good stability. The phosphor layer can effectively prolong the service life of batteries, and even improve the
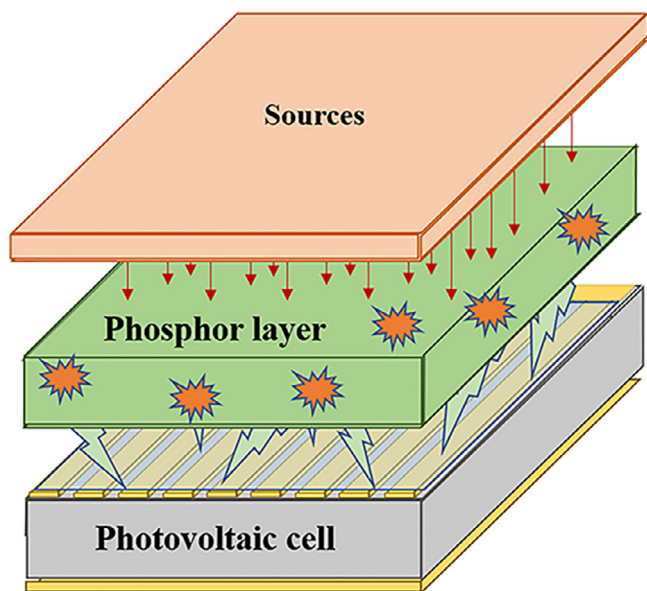
FIGURE 1 The structure of the radioluminescent nuclear battery [Colour figure can be viewed at wileyonlinelibrary.com]

output power.[11-14] Research on radioluminescent nuclear battery mainly focuses on the optimized design of phosphor and the structure of phosphor layers. The electrical property of it can be enhanced by matching the quantum efficiency of the photovoltaic unit and increasing the emission photon of the phosphor layer.[15-17] These findings extend the potential application of nuclear battery. ZnS-based fluorescent materials have excellent properties for the radioluminescent nuclear battery, and extensive research has been carried out based on this material.[18-20] In addition, the coupling of radioisotope sources and fluorescent materials is also the main way to improve the property. There greatly enhance the utilization of radioisotopes and emission photons by using a liquid source and fluorescent.[20] Variety of the phosphor and the substrate under the same radiation source will also impact on the photon emission of phosphor layers.[21] The phosphor layer is a planar structure sandwiched between the radioisotope source and the photovoltaic unit. It is necessary to ensure that the decay energy is completely deposited and sufficient radioluminescence photons are emitted. Therefore, the design and optimization of phosphor layer is a crucial item to study radioluminescent nuclear battery. This paper is a present study on ZnS:(Cu, Al) phosphor, which focuses on the coupling of radioisotope sources and phosphor layers, and explores variation tendency of properties after irradiation.

This work has explored the luminescence enhancement of ZnS:(Cu, Al) phosphor layer at the microscale in accordance with the γ radiation optimization of the nanoscale quantum dot fluorescent materials.[22-24]

ZnS-based phosphors are oxidized, discolored, and have a larger grain size due to electron radiation.[25-27] However, there was little work that investigated the micromorphology, optical, and electrical properties of ZnS:(Cu, Al) phosphors after high-dose electron radiation. The combination of simulation and experiment is a suitable method to analyze the effect of radioactive particles on materials.[28,29] It is meaningful for exploring the performance changes and micromechanism of energy conversion section after radiation in batteries, providing important guideline for predicting battery service behavior. All of these studies play a certain role in the optimization and preparation of phosphor layers and property evaluation of radioluminescent nuclear battery.

2 | MATERIALS AND METHODS

2.1 | Monte Carlo simulation

The energy deposition of ZnS:(Cu, Al) was simulated by MCNP5 and counted by *F8 card. Absorbed dose (D) is the quotient of $d\varepsilon$ by dm, where $d\varepsilon$ is the mean deposited energy imparted by ionizing radiation to matter of incremental mass dm. The absorbed dose can be obtained by:

$$D = d\varepsilon / dm. \quad (1)$$

In Monte Carlo simulation, the material was layered to obtain absorbed dose at different depths. The dose rate of the electron accelerator was the surface layer of ZnS:(Cu, Al), and it would change as the increasing thickness. Therefore, the thickness of phosphor for the radiation experiment should be simulated to accurately calculate the absorbed dose. The simulation model was an electron source with 10 MeV, and the irradiated material was divided into 30 mm × 30 mm × 0.1 mm per layer. The number of simulated electrons was 109; the relative error was less than 0.15%. The structure and the result are shown in Figure 2.

Figure 2B is the trend of energy deposition and absorbed dose with increasing thickness. The yellow line represents the absorbed dose and the gray column is the energy deposition. The energy deposition gradually increased with the thickness of the phosphor, and the rate of increase rose and then decreased. It is because high-energy electrons generate bremsstrahlung and secondary electrons in phosphor. The absorbed dose of ZnS:(Cu, Al) at the thickness of 11.9 mm is equal to the surface layer. Therefore, the thickness of 11.9 mm was used for sample positioning in irradiation experiments.
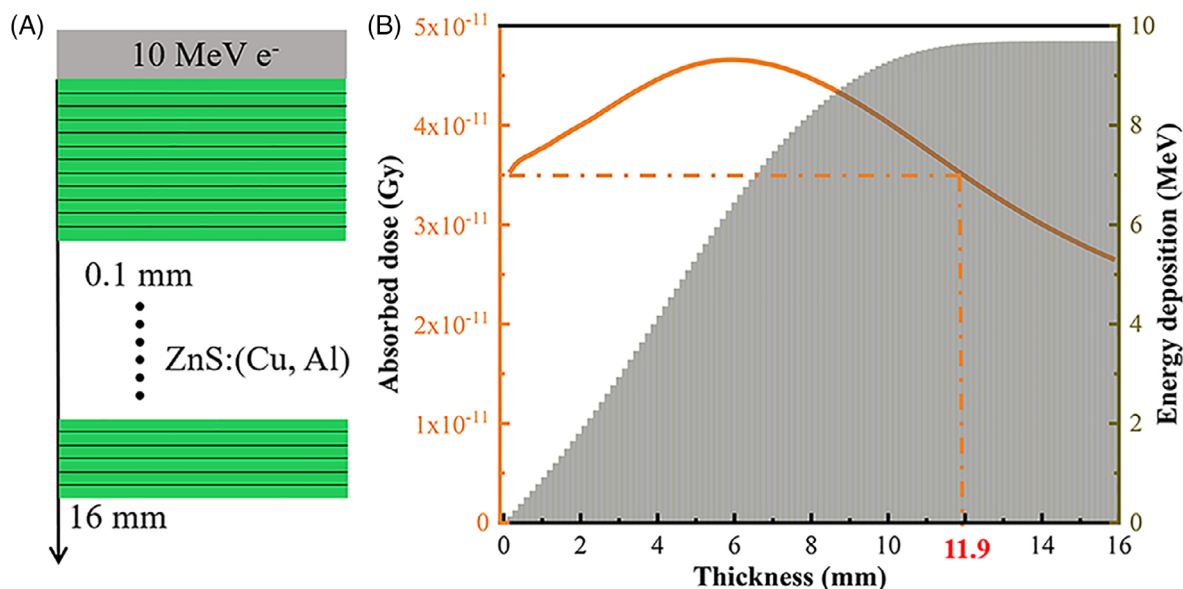
FIGURE 2   A, Structural design in MCNP5 simulation; B, Simulation result of energy deposition and absorbed dose in phosphor [Colour figure can be viewed at wileyonlinelibrary.com]

2.2 | Experimental procedure

2.2.1 | Radiation condition

The γ radiation experiment of the phosphor layer was conducted with a high activity ^{60}Co radioisotope source whose dose rate is 12.4 kGy/h (^{60}Co Radiation Center of Nanjing University of Aeronautics and Astronautics).

High-dose β radiation experiments of ZnS:(Cu, Al) phosphors were carried out with an electron accelerator, whose energy is 10 MeV and surface absorbed dose rate is 19 kGy/s (Dasheng Electron Accelerator). The dose rate of the β particles emitted by electron accelerator is the value on surface layer, so the dose rate in-depth needs to be simulated by Monte Carlo.

2.2.2 | Characterization and property testing

The property variation of the phosphor was analyzed after irradiation. The optical property and radioluminescence spectra were obtained using Agilent Technologies Cary Eclipse fluorescence spectrophotometer. The electrical property of the radioluminescent nuclear batteries was evaluated by a source meter (Keithley 2636A). The photoelectric conversion device of the radioluminescence is AlGaInP semiconductor photovoltaic units, whose quantum efficiency has a good matching with the emission spectrum of ZnS:(Cu, Al). X-ray diffraction (XRD) was used to analyze the crystal structure of the phosphor. Surface morphology was studied using a scanning electron microscope (SEM).

2.2.3 | Phosphor layer preparation

There are two methods of preparation of phosphor layer: "adhesion" method and "blending" method. The "adhesion" phosphor layer consists of two parts: fluorescent material layer and substrate layer. The fluorescent material layer is the single-grain phosphor with the size of 5 μm. The substrate layer is the biaxially oriented polypropylene (BOPP) with the thickness of 50 μm. The ZnS:(Cu, Al) phosphor grains were directly adhered on the BOPP substrate, and thinned to single-grain phosphor adhesion. The "blending method" phosphor layer blended the fluorescent material with silicone. Glue and hardener (high transparent silica gel) were weighed into a Teflon beaker at a ratio of 1:1, stirred for 0.5 hour, mixed well, added with a certain amount of fluorescent material, and then placed into a vacuum defoamer. The silicone and fluorescent material were mixed into the casting machine tank, the thickness was controlled at 150 μm, and the substrate was coated. The plated film substrate was placed in the oven, which was maintained at 60°C for 1 hour and at 150°C for 3 hours. The film was peeled off from the substrate to obtain the "blending" phosphor layer.

3 | RESULTS AND DISCUSSION

3.1 | Coupling and optimized preparation of phosphor layer

"Adhesion" phosphor layer is usually used for β-radioluminescent nuclear battery. β sources deposit energy

completely in a shallow layer, so the close contact between radioisotope sources and phosphor is an efficient energy conversion method. Meanwhile, a thicker phosphor layer will cause more self-absorption of radioluminescence photons, and a thinner phosphor layer will cause a loss of radiation source energy. It is believed that the thickness of the phosphor is equal to the energy deposition depth of the radioactive particles is the best coupling solution.

3.1.1 | Coupling of radiation source and phosphor layer

The simulation result of the energy deposition of ^{63}Ni and ^{147}Pm radioisotope source in the ZnS:(Cu, Al) phosphor is shown in Figure 3.

It is shown that the thickness of the single-grain phosphor is sufficient to deposit most energy of ^{63}Ni radioisotope. Because of the higher emission energy of ^{147}Pm, its penetration depth is deeper than ^{63}Ni. Single-grain phosphor cannot completely absorb the electron energy, causing not only energy loss but also unnecessary damages on the substrate layer. ^{63}Ni radioisotope source is an excellent combination scheme of the "adhesion" phosphor layer in this work. And ^{147}Pm radioisotope source is fit for a phosphor with grain size of 50 μm.

3.1.2 | Electrical property of the batteries with different phosphor layers

An X-ray generator was used for equivalent γ radioisotope sources. The analysis of the maximum power (P_{max}) of two phosphor layer batteries under shifty voltages is shown in Figure 4, which the current was fixed at 400 μA.

The output power has an obvious enhancement trend with increasing voltage. The output power of two phosphor layer batteries was almost the same when the X-ray generator voltage was 10 kV. As the voltage rose, the enhancement trend of output power of "blending" phosphor layer batteries was significantly higher than that of the "adhesion" phosphor layer batteries. Besides, the increasing rate of the P_{max} of "adhesion" phosphor layer batteries gradually slows down with the enhancement voltage. The result indicates that "blending" phosphor layer battery will have a better electrical property under low liner energy transfer radioisotope sources such as ^{60}Co, ^{137}Cs, or other γ-radioisotope sources. The higher the energy of the γ particles the greater advantage of the "blending" phosphor layer because it contains more phosphor grains and a mass of radioluminescence photons can be excited by the γ ray. Therefore, γ-radioluminescent nuclear batteries use "blending" phosphor layers to perform better energy conversion and obtain higher power output.

3.1.3 | γ-radiation enhanced luminescence of the phosphor layer

The two kinds of phosphor layers irradiated by ^{60}Co were loaded into the radioluminescent nuclear battery with different particle sources. The trend of electrical properties with increasing radiation dose is shown in Figure 5.

The red and black data points in Figure 5 reflect the results of multiple measurements; the blue and yellow
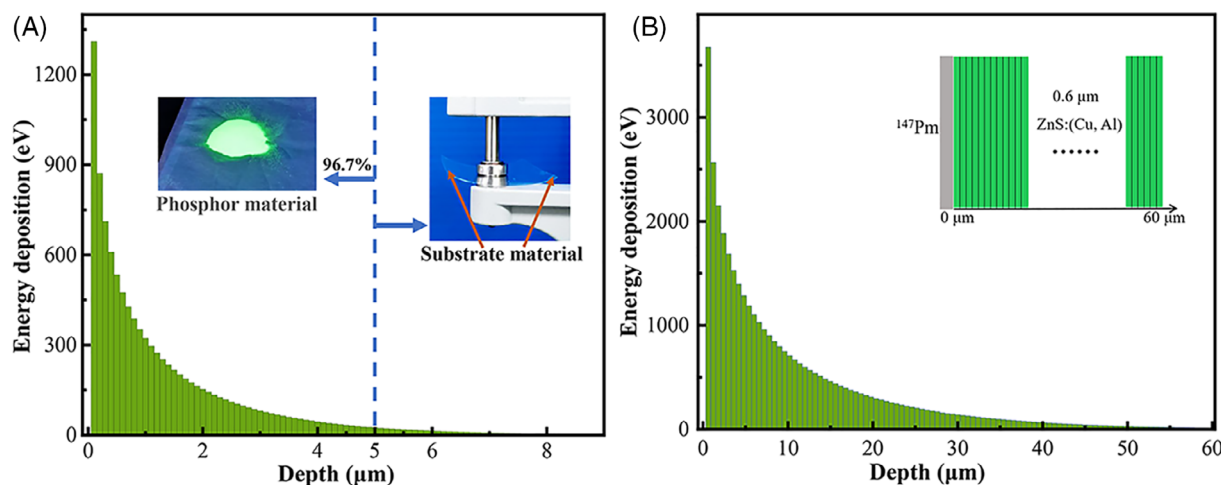
FIGURE 3 A, Energy deposition of ^{63}Ni radioisotope; B, Energy deposition of ^{147}Pm radioisotope [Colour figure can be viewed at wileyonlinelibrary.com]

shadow represents the average value of the results. The P_{max} and short-circuit current (I_{sc}) were increasing after the ^{60}Co γ radiation. The same change trend of P_{max} and I_{sc} indicated that the open-circuit voltage (V_{oc}) and fill factor (FF) were stable, so the electrical property of battery was only related to the number of emission photons from the phosphor layer. The photon yield of phosphor layers was enhanced under γ radiation. The radiation enhancement effect of the "blending" phosphor layer reached a peak increasing by 46% when the radiation dose was 348.4 kGy, and then radioluminescence photon yield decreased slightly with the increasing radiation dose. This is a result of the competitive relationship between the radiation damage effect and the radiation enhancement effect. The "adhesion" phosphor layer increased continually, and had a 50% increase at the dose

of 871 kGy. Hence, γ radiation processing is an effective way to enhance radioluminescence intensity of the phosphor layer.

3.2 | Electron irradiation stability of phosphor

The phosphor with the thickness of 11.9 mm was placed in aluminum boxes in the electron radiation experiment. The phosphor with electron radiation was prepared into phosphor layers by "adhesion" method for optical and electrical property testing.

3.2.1 | Optical property

^{63}Ni was loaded as the radioisotope source to excite phosphor layer. The radioluminescence spectrum is shown in Figure 6A. The luminescence integral intensity of the phosphors irradiated is shown in Figure 6B.

The peak of the emission wavelength of different radiation doses of phosphors shows no significant shift. The wavelength range of the radioluminescence is still between 450 and 650 nm. There is no spectral excursion in the phosphor, but the number of emission photon is reduced due to radiation defects. The luminescence intensity of the phosphor decreases gradually with increasing radiation dose. The decay rate is initially fast and then slows down. The attenuation tends to be stable between 5.14 and 6.85 MGy. Another significant attenuation occurs at the dose of 8.56 MGy, and the fluorescence intensity is decreased by 49.5%. The specific attenuation mechanism needs further analysis through microscopic characterization.
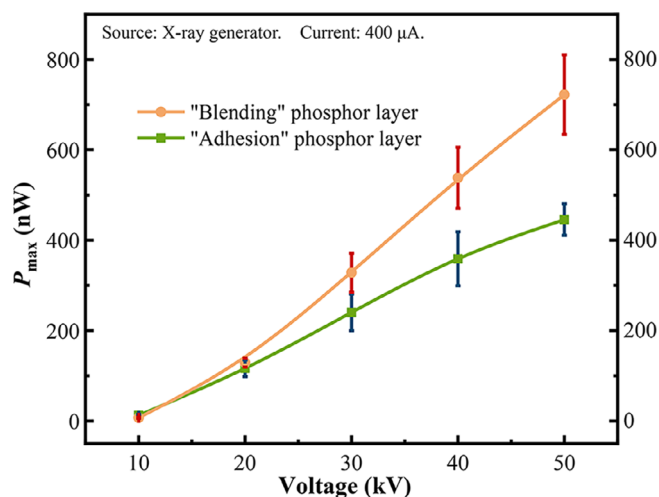
FIGURE 4 Maximum power of radioluminescent nuclear batteries with increasing voltage of X-ray generator [Colour figure can be viewed at wileyonlinelibrary.com]
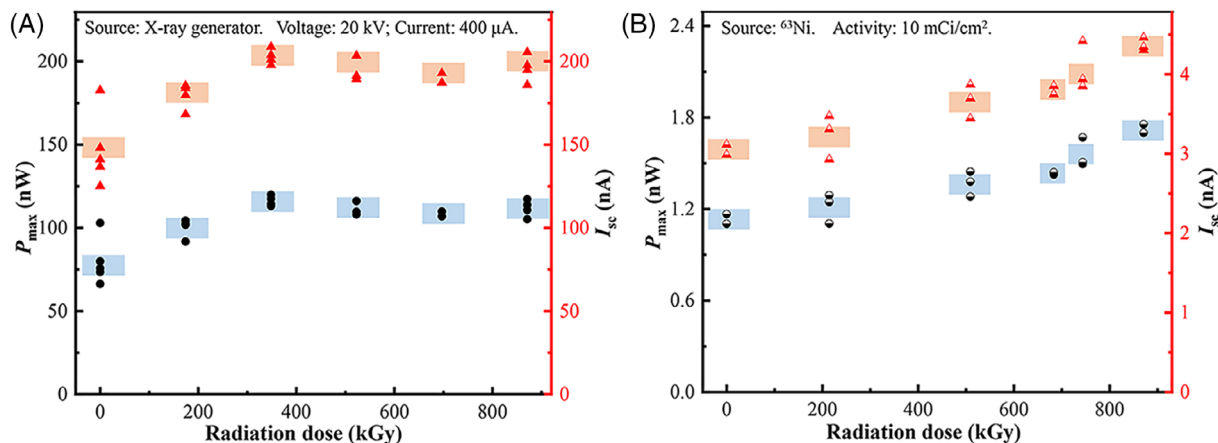
FIGURE 5 The electrical properties with increasing γ radiation dose A, "blending" phosphor layer; B, "adhesion" phosphor layer [Colour figure can be viewed at wileyonlinelibrary.com]
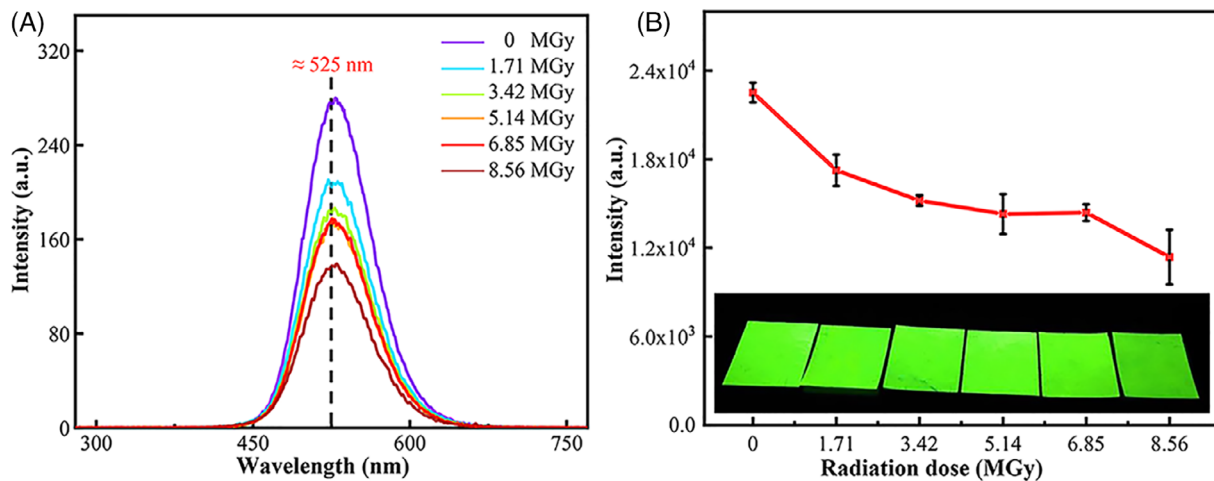
FIGURE 6 A, Radioluminescence spectra of phosphors after electron radiation; B, Optical properties trend of phosphors after electron radiation [Colour figure can be viewed at wileyonlinelibrary.com]

TABLE 1 Electrical parameters after irradiation at different doses

Dose (MGy)	I_{sc} (nA)	V_{oc} (V)	P_{max} (nW)	FF
0	3.88	0.61	1.29	0.534
1.71	3.47	0.59	1.14	0.557
3.42	3.30	0.59	1.08	0.552
5.14	3.15	0.63	0.96	0.480
6.85	2.96	0.63	0.94	0.501
8.56	2.41	0.59	0.73	0.515

3.2.2 | Electrical property

The ^{63}Ni was loaded on the upper part of the 30 mm × 30 mm "adhesion" phosphor layer, and an 11 mm × 11 mm AlGaInP semiconductor photovoltaic unit was used for photoelectric conversion. The electrical output parameters are shown in Table 1. The attenuation trend of P_{max} is shown in Figure 7.

The FF and V_{oc} are only slightly fluctuated without obvious variation tendency, and the attenuation trend of I_{sc} and P_{max} is similar to that of the optical properties of phosphor. The result indicates that the property of the radioluminescent nuclear battery is mainly depending on emission radioluminescence of the phosphor layer. When the absorbed dose reached 8.56 MGy, the output power of the battery dropped by 43.4%. Electron radiation on the phosphor caused radiation damage that decreased the photon yield of it. The incident photons of the semiconductor photovoltaic unit reduced; the current decreased, resulting in a decreasing output power of the battery. Specific electron radiation damage and accompanying changes at the microscopic level require further microscopic characterization.

3.2.3 | Crystal structure

Figure 8 shows the XRD patterns of the phosphor. Figure 8A compares the initial phosphor with the standard PDF card of ZnS, and Figure 8B compares the phosphor with different radiation dose.

According to the comparison with the standard PDF card of ZnS, the diffraction peaks of the two are consistent, indicating that the main component of this phosphor is ZnS. The elemental composition, crystal plane orientation, and grain structure of the phosphor did not change after electron radiation. In addition, the full-width half maximum (FWHM) is very narrow, indicating that the irradiated phosphor still had good crystallinity. The grain size changed continuously, and no phase transition or interplanar spacing change occurred. The anti-radiation performance of ZnS:(Cu, Al) is excellent, but some regular heterogeneous phases appeared near the (111) crystal plane, electron radiation caused some defects in its crystal structure. No other components were introduced here; it was still the ZnS:(Cu, Al) phosphor that played the role of absorbing electrons to emit luminescence. The emission decay is caused by the crystal grain defects of the phosphor itself.

3.2.4 | Surface morphology

The defect effect and surface morphology of phosphor after radiation was analyzed. Figure 9 shows the SEM images of the morphological characteristics of the microscopic surface of irradiated phosphors.

There were more defects generated on the grain surface as the increasing absorbed dose. The defects on the surface of phosphor acted as a light trap to self-absorb
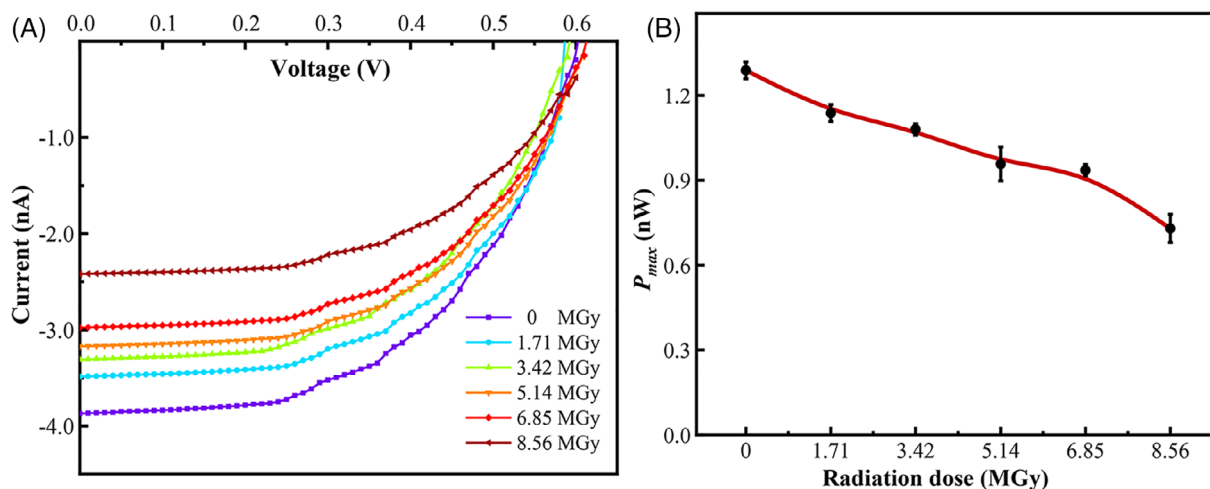
FIGURE 7 A, *I-V* curve of electrical properties after electron radiation; B, Trend of P_{max} after electron radiation [Colour figure can be viewed at wileyonlinelibrary.com]
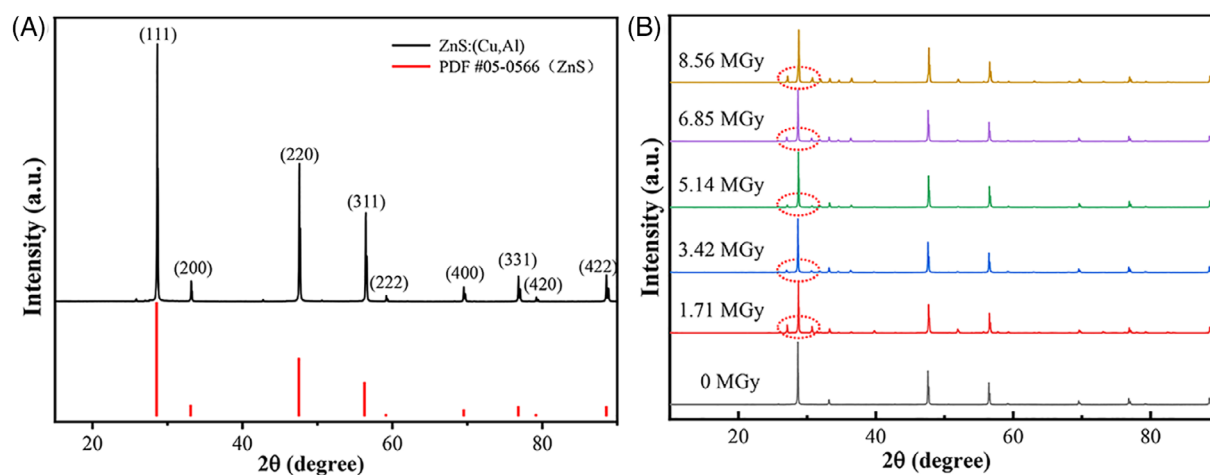
FIGURE 8 A, Comparison of phosphor with standard PDF cards; B, XRD patterns of phosphors after electron radiation [Colour figure can be viewed at wileyonlinelibrary.com]

the radioluminescence photons, causing ZnS:(Cu, Al) phosphor to lose its energy level transition. One hundred grains were randomly selected from the SEM image for grain size statistics, shown in Figure 10.

The initial phosphor grain size is 5.14 μm. At electron radiation dose of 8.56 MGy, the ZnS:(Cu, Al) grain size increased to 8.59 μm, which increased by 67.1%. The size of the crystal grains meets the Gaussian distribution. As the electron radiation dose increases, the broadening becomes larger and the grain size distribution becomes dispersed. According to previous research, it can be known that a bigger size of phosphors will lead to a higher luminous intensity.[12,30] However, it occurs a significant decrease in luminous intensity at large sizes. It is inferred that the decrease in performance is due to the swelling of the grains and the generation of defect voids, combined with surface hole defects observed in SEM images.[25,26] The growth grain size of the phosphor is due

to the thermal effect produced by high-energy electron radiation, which causes the crystal of the phosphor to recrystallize and accumulate the point defects on the crystal plane. The kinetic energy obtained by the effect of external electrons on the atom and the proper lattice position is occupied, thereby transforming the crystal. The rearrangement changes the grain size. The increased number of interacting electrons transfers energy to the dislocated atoms, which shifts and reorganizes the lattice. Many atoms even attach to the ZnS, increasing the average size of the crystal.

4 | CONCLUSIONS

The study explored the coupling of the phosphor layer with the radioisotope source, and analyzed the radiation damage of the phosphor. The γ-radioluminescent
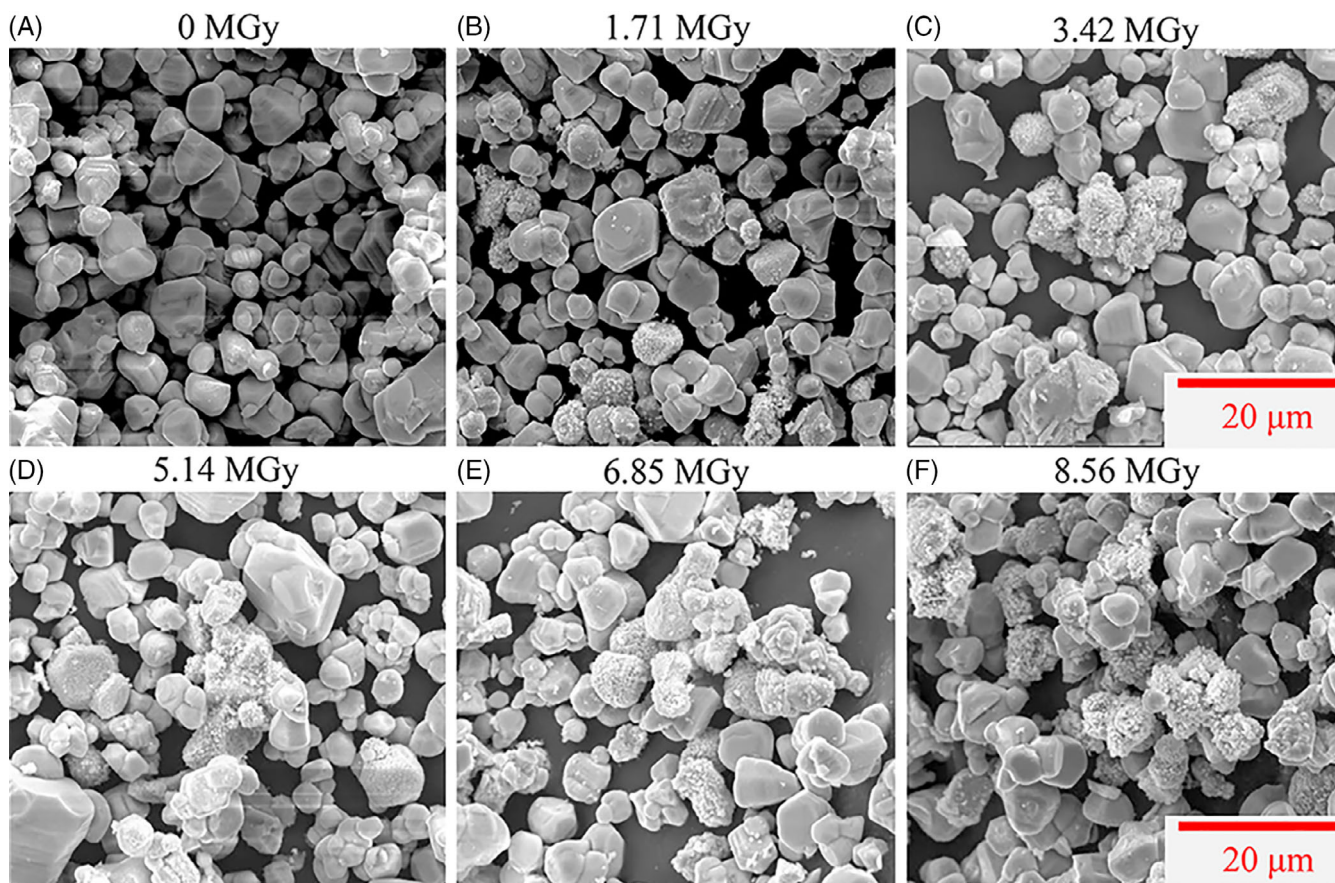
FIGURE 9   SEM of phosphors after electron radiation [Colour figure can be viewed at wileyonlinelibrary.com]
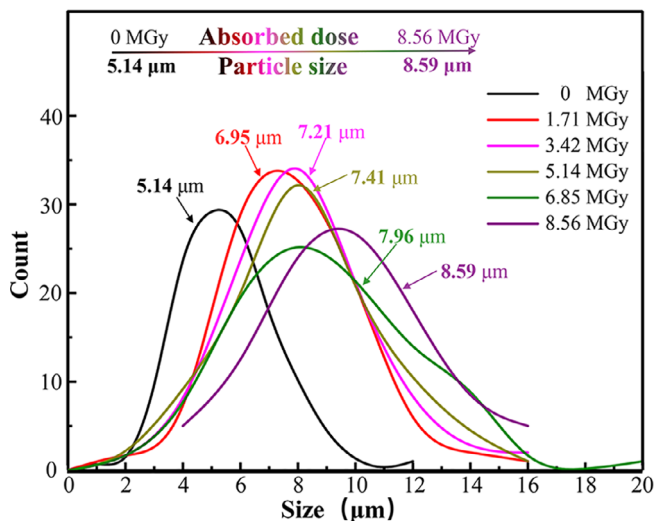
FIGURE 10   Grain size growth of phosphors after electron radiation [Colour figure can be viewed at wileyonlinelibrary.com]

nuclear battery and the "blending" phosphor layer are a combination of higher output power. And the β-radioluminescent nuclear battery matching "adhesion" phosphor layer has better service stability. Moreover, both of the phosphor layers irradiated by ^{60}Co γ-radiation occurs a radioluminescence enhancement. The increased electrical property of "blending" phosphor layer will meet a peak by about 146% when the radiation dose reaches 348.4 kGy, and then decreased slightly with increasing radiation dose. The property of "adhesion" phosphor layer continues to increase even if the radiation dose reaches 871 kGy; it has risen by 50%. Evaluation for the stability of phosphor layer service property shows that the point defects caused by electron radiation lead to a larger grain size and a lower emission photon. The radioluminescence intensity of it decreased by 50%, and the P_{max} of β nuclear battery decreased by 43% when the absorbed dose reached 8.56 MGy. The ZnS:(Cu, Al) phosphor layer structure of two kinds of ray-type nuclear battery have great radiation resistance, which predicts the battery have stable output power over a long time, and the application field can be extended in harsh radiation environments. The luminescence enhancement of phosphor layers by γ irradiation is of great significance for increasing the output power of radioluminescent nuclear battery. It is necessary to analyze the inherent optimization mechanism in the further study.

ORCID

Xiaobin Tang https://orcid.org/0000-0003-3308-0468

REFERENCES

1. Bower KE, Barbanel YA, Shreter YG, Bohnert GW. *Polymers, Phosphors, and Voltaics for Radioisotope Microbatteries*. Boca Raton: CRC Press; 2002:35-51.
2. Yakubova, Galina N. Nuclear batteries with tritium and promethium-147 radioactive sources. Diss. University of Illinois at Urbana-Champaign, 2010.
3. Landis GA, Bailey SG, Clark EB, Myers MG, Piszczor MF, Murbach MS. Non-solar photovoltaics for small space missions. Paper presented at: 2012 38th IEEE Photovoltaic Specialists Conference. IEEE, 2012.
4. Prelas MA, Weaver CL, Watermann ML, Lukosi ED, Schott RJ, Wisniewski DA. A review of nuclear batteries. *Prog Nucl Energy*. 2014;75:117-148.
5. Walko, R. J., et al. Electronic and photonic power applications. No. SAND-90-2130C; CONF-9009201–1. Sandia National Labs., Albuquerque, NM (USA), 1990.
6. Bailey, Sheila G., et al. Photovoltaic development for alpha voltaic batteries. Paper presented at: Conference Record of the Thirty-first IEEE Photovoltaic Specialists Conference. IEEE, 2005.
7. Aydin S, Kam E. Investigation of nickel-63 radioisotope-powered GaN betavoltaic nuclear battery. *Int J Energy Res*. 2019;43(14):8725-8738.
8. Liu B, Liu K, Ralchenko V, et al. Effect of americium-241 source activity on total conversion efficiency of diamond alpha-voltaic battery. *Int J Energy Res*. 2019;43(11):6038-6044.
9. Sychov M, Kavetsky A, Yakubova G, et al. Alpha indirect conversion radioisotope power source. *Appl Radiat Isot*. 2008;66 (2):173-177.
10. Cress CD, Redino CS, Landi BJ, Raffaelle RP. Alpha-particle-induced luminescence of rare-earth-doped Y_2O_3 nanophosphors. *J Solid State Chem*. 2008;181(8):2041-2045.
11. Zhang Z, Tang X, Liu Y, et al. Use the indirect energy conversion of the phosphor layer to improve the performance of nuclear batteries. *Energ Technol*. 2018;6(10):1959-1965.
12. Tang X, Xu Z, Liu Y, Liu M, Wang H, Chen D. Physical parameters of phosphor layers and their effects on the device properties of Beta-radioluminescent nuclear batteries. *Energy Technol*. 2015;3(11):1121-1129.
13. Xu Z et al. Development of a beta radioluminescence nuclear battery. *Nucl Sci Tech*. 2014;25(4).
14. Zhang Z-R et al. GaAs radiovoltaic cell enhanced by Y_2SiO_5 crystal for the development of new gamma microbatteries. *Nucl Instrum Methods Phys Res, Sect B*. 2017;398:35-41.
15. Chen, Wang, et al. "Novel radioluminescent nuclear battery: spectral regulation of perovskite quantum dots." *Int J Energy Res* 42.7 (2018): 2507–2517.
16. Guo X, Liu Y, Xu Z, et al. Multi-level radioisotope batteries based on ^{60}Co γ source and radio-voltaic/radio-photovoltaic dual effects. *Sens. Actuators, A*. 2018;275:119-128.
17. Xu Z, Liu Y, Zhang Z, et al. Enhanced radioluminescent nuclear battery by optimizing structural design of the phosphor layer. *Int J Energy Res*. 2018;42(12):1729-1737.
18. Hong L et al. Radioluminescent nuclear batteries with different phosphor layers. *Nucl Instrum Methods Phys Res, Sect B*. 2014; 338:112-118.
19. Xu Z, Tang X, Liu Y, et al. ZnS: cu phosphor layers as energy conversion materials for nuclear batteries: a combined theoretical and experimental study of their geometric structure. *Energ Technol*. 2017;5(9):1638-1646.
20. Russo J, Litz M, Ray W, Smith B, Moyers R. A radioluminescent nuclear battery using volumetric configuration: ^{63}Ni solution/ZnS: Cu, Al/InGaP. *Appl Radiat Isot*. 2017;130: 66-74.
21. Yürük RK, Tütüncüler H. Investigation of the effect of beta source and phosphors on photovoltaic cells. *AIP Conf Proc*. 2017, February;1815(1):040002.
22. Chang, Shuquan, et al. "γ-Radiation enhanced luminescence of Thiol-capped quantum dots in aqueous solution." *Nanomaterials* 9.4 (2019): 506.
23. Zhang Y, Zhu H, Huang T, Song Z, Ruan S. Radiation-pressure-induced photoluminescence enhancement of all-inorganic perovskite $CsPbBr_3$ quantum dots. *Photonics Res*. 2019;7(8): 837-846.
24. Masoud EM, Abdelazeem ES. Enhanced properties of gamma irradiated nano spinels containing cobalt and aluminum ions: effect of gamma radiation on structure, electrical, magnetic and thermal stability properties. *Ionics*. 2019;25(2):835-847.
25. Oosthuizen L et al. ZnS: cu, Al, au phosphor degradation under electron excitation. *Appl Surf Sci*. 1997;120(1–2):9-14.
26. Priya K, Rao GK, Ashith VK, et al. The effect of 8 MeV electron beam irradiation on the structural, optical and photoluminescence properties of ZnS thin films. *Ceram Int*. 2019;45 (2):2576-2583.
27. Brunner S et al. Induced defects in ZnS by electron and proton irradiation and defect-annealing behavior. *Physica B*. 1999;273: 898-901.
28. Wu H, Xie Z, Wang Y, et al. A constitutive model coupling irradiation with two-phase lithiation for lithium-ion battery electrodes. *Philos Mag*. 2019;99(8):992-1013.
29. Ma Z, Wu H, Wang Y, Pan Y, Lu C. An electrochemical-irradiated plasticity model for metallic electrodes in lithium-ion batteries. *Int J Plast*. 2017;88:188-203.
30. Igarashi T, Isobe T, Senna M. EPR study of Mn^{2+} electronic states for the nanosized ZnS: Mn powder modified by acrylic acid. *Phys Rev B*. 1997;56(11):6444.